nature structural & molecular biology

RdRP-synthesized antisense ribosomal siRNAs silence pre-rRNA via the nuclear RNAi pathway

Xufei Zhou[1,2], Xuezhu Feng[1,2], Hui Mao[1], Mu Li[1], Fei Xu[1], Kai Hu[1] & Shouhong Guang[1]

Expression of rRNA affects cell growth and proliferation, but mechanisms that modulate rRNA levels are poorly understood. We conducted a genetic screen for factors that negatively regulate generation of endogenous short interfering RNA (endo-siRNA) in *Caenorhabditis elegans* and identified a suppressor of siRNA (*susi-1*) and antisense ribosomal siRNAs (risiRNAs). risiRNAs show sequence complementary to 18S and 26S rRNAs and require RNA-dependent RNA polymerases (RdRPs) for their production. They act through the nuclear RNA interference (RNAi) pathway to downregulate pre-rRNA. Stress stimuli, including low temperature and UV irradiation, induced the accumulation of risiRNAs. SUSI-1 is a homolog of the human DIS3L2 exonuclease involved in 3′–5′ degradation of oligouridylated RNAs. In *susi-1* mutant and in low temperature-treated animals, 3′-tail oligouridylated 26S rRNA accumulated. The injection of oligouridylated rRNA elicited nuclear accumulation of NRDE-3. Our findings identify a new subset of 22G-RNAs that regulate pre-rRNA expression and a mechanism to maintain rRNA homeostasis.

Argonaute proteins have central roles in small RNA–mediated gene regulation. Diverse pathways have been implicated in the biogenesis and loading of small RNA species onto their respective Argonaute proteins[1–4]. Small regulatory RNAs can be categorized into distinct classes—such as microRNA, PIWI-interacting RNA (piRNA) or endo-siRNA)—according to their mechanism of biogenesis, mode of regulation or the particular Argonaute protein they interact with.

Small regulatory RNAs can be generated from targeted RNA by RdRPs to amplify the silencing effects of RNAi[5–8]. In nematodes, RdRPs catalyze the unprimed, *de novo* synthesis of 5′-triphosphorylated RNAs, which are loaded onto worm-specific Argonaute proteins (WAGOs)[8–12]. Because these secondary siRNAs have a strong propensity for a 5′ G residue and are 22 nt long, they are termed 22G-RNAs.

Many genes are involved in the production of 22G-RNAs[5,12–16]. However, it is unclear how a particular nucleic acid sequence is selected to direct endo-siRNA generation. Endo-siRNAs can be derived from loci capable of double-stranded RNA (dsRNA) formation[1,3]. In *C. elegans*, endo-siRNAs are produced from both repetitive and unique nucleic acid sequences[17]. The endoribonuclease RDE-8 is recruited to targeted mRNA by RDE-1, cleaves mRNA and enables 3′ uridylation of the mRNA fragment. These processes are required to promote RdRP activity and ensure amplification of 22G-RNA[5]. NRDE-3 binds endo-siRNAs mainly from repetitive loci[18].

We conducted a genetic screen for factors that negatively regulate endo-siRNA production in *C. elegans* and identified risiRNAs that are antisense to 18S and 26S rRNAs and the suppressor of siRNA SUSI-1. risiRNAs act, at least in part, through the nuclear RNAi pathway to downregulate pre-rRNA. Various stress stimuli can increase risiRNA accumulation. Cloned SUSI-1 shows homology to human DIS3L2. Using a TAIL-seq assay to sequence the very end of rRNA molecules, we observed an accumulation of oligouridylated 26S rRNA in a *C. elegans susi-1*(*ceDIS3L2*) mutant and low-temperature-treated animals. Our findings thus establish SUSI-1(ceDIS3L2) as a suppressor of risiRNA generation and identify an risiRNA that downregulates rRNA expression.

RESULTS

risiRNA accumulates in the *susi-1* mutant

NRDE-3 localizes to the nucleus when it binds to siRNAs but accumulates in the cytoplasm in the absence of siRNA ligands[14]. Impairments of the generation of endogenous siRNA relocalize NRDE-3 from the nucleus to the cytoplasm, as seen in *eri*, *mut* and *rrf* mutants (**Fig. 1a**). The *eri*, *mut* and *rrf* genes are each required for the production of distinct class of endo-siRNAs.

We designed genetic screening strategies to search for negative factors of endo-siRNA production in *C. elegans*. We chemically mutagenized *eri-1(mg366);gfp::nrde-3* worms, in which NRDE-3 localizes to the cytoplasm, and searched for mutants that were capable of redistributing NRDE-3 from the cytoplasm to the nucleus by clonal screening. We isolated eight *susi* mutants from 8,000 haploid genomes. One *susi-1* allele was isolated from this screening. In *eri-1(mg366);gfp::nrde-3*, NRDE-3 accumulated in the cytoplasm, whereas in *eri-1(mg366);susi-1(ust1);gfp::nrde-3*, NRDE-3 relocalized to the nucleus (**Fig. 1b**). Notably, NRDE-3 also accumulated in nucleoli in mutant embryos. We exogenously provided a variety of dsRNAs to *C. elegans* and found that SUSI-1 had a marginal, if any, direct role in feeding RNAi (**Supplementary Table 1**).

We immunoprecipitated NRDE-3 and labeled the bound RNA with ^{32}P. NRDE-3 bound endo-siRNA in wild-type (N2) worms but

[1]School of Life Sciences, CAS Center for Excellence in Molecular Cell Science, University of Science and Technology of China, Hefei, China. [2]These authors contributed equally to this work. Correspondence should be addressed to S.G. (sguang@ustc.edu.cn).

Received 25 June 2016; accepted 10 January 2017; published online 6 February 2017; doi:10.1038/nsmb.3376

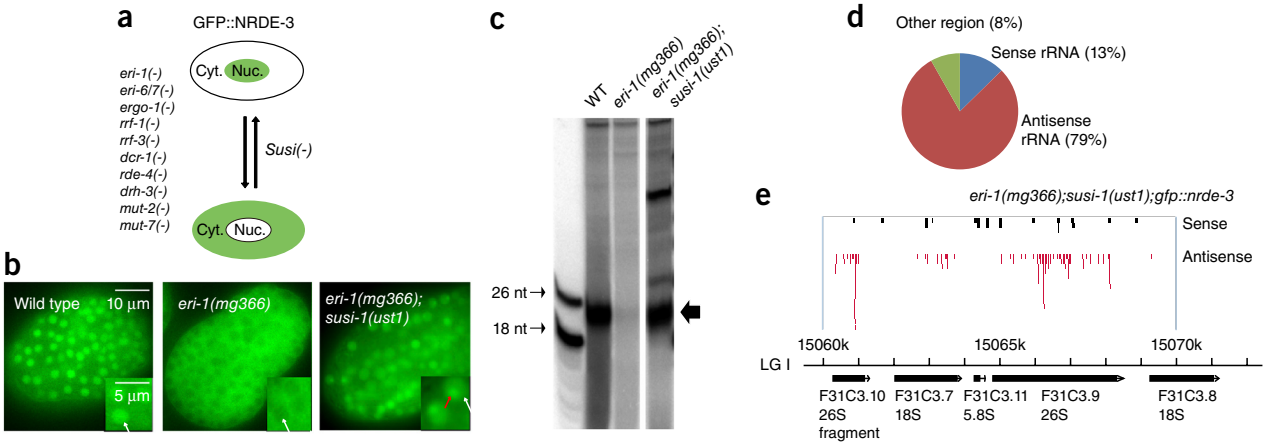

Figure 1 Accumulation of risiRNA in the suppressor of siRNA *susi-1* mutant. (**a**) Subcellular localization of NRDE-3 was used as a reporter to screen for suppressors of mutants in endo-siRNA generation. Cyt., cytoplasm; nuc., nucleus. (**b**) Images of *C. elegans* embryos with the indicated genotypes expressing GFP::NRDE-3 at the ~300-cell stage. White arrows, nucleus; red arrow, nucleoli. (**c**) NRDE-3-associated small RNAs from the indicated strains were immunoprecipitated, labeled with ^{32}P and resolved by gel electrophoresis. The uncropped gel image is shown in **Supplementary Data Set 1**. WT, wild type. (**d**) Distribution of NRDE-3-associated siRNAs isolated by immunoprecipitation and manual cloning. (**e**) Strand distribution of NRDE-3-associated siRNAs corresponding to the rDNA locus.

not in *eri-1(mg366)* mutants[14]. In *eri-1(mg366);susi-1(ust1);gfp::nrde-3* animals, NRDE-3 reassociated with small RNAs 20–22 nt in length (**Fig. 1c** and **Supplementary Data Set 1**).

We manually cloned 151 RNAs (~20–22 nt long) that were in complex with NRDE-3 *in vivo* from *eri-1(mg366);susi-1(ust1);gfp::nrde-3* animals (**Supplementary Table 2**). Notably, 79% of the NRDE-3-associated small RNAs showed sequence complementarity to 18S and 26S rRNAs (**Fig. 1d**,**e**). Small rRNAs have long been viewed as degradation products and thus are usually discarded during high-throughput RNA-seq analyses. The identification of risiRNAs, together with their ability to bind and redistribute the Argonaute protein NRDE-3, suggests potential regulatory functions.

risiRNA is a subclass of 22G-RNA

We explored whether risiRNA belongs to a known class of endogenous small RNAs. First, we deep sequenced small RNAs of 18–30 nt in length from wild-type N2 and *susi-1(R457H)* animals and selected rRNA-related small RNA sequences. The allele encoding R457H substitution in SUSI-1 also induced redistribution of NRDE-3 to the nucleus (see below). The numbers of sense rRNA reads were similar between wild-type and *susi-1(R457H)* samples (**Supplementary Fig. 1a**), and these rRNAs were random in size and did not show a propensity for a particular 5′ end nucleotide (**Supplementary Fig. 1b**), which was consistent with the prediction of rRNA degradation. Yet the abundance of risiRNA reads was approximately ten-fold higher in *susi-1(R457H)* (**Fig. 2a**,**b**). The majority of risiRNAs started with a guanidine at the 5′ end and were 22 nt in length, which suggests they are 22G-RNAs (**Fig. 2b**).

We compared other small RNA categories in *susi-1(R457H)* and wild type N2 (**Supplementary Fig. 1c**,**d**). SUSI-1 is probably required for the accumulation of some endo-siRNAs, piRNAs and microRNAs, but here we focused on the role of SUSI-1 in suppressing risiRNA generation.

To test whether risiRNAs bind to Argonaute proteins besides NRDE-3, we analyzed published data sets of Argonaute-bound small RNAs[18] (**Fig. 2c**,**d** and **Supplementary Fig. 2a**). These Argonaute proteins were immunoprecipitated from the wild-type N2 background and deep sequenced in a 5′ P–independent method. risiRNAs were also present in WAGO-1, CSR-1 and HRDE-1 immunoprecipitates[12,19–21].

Next, we characterized the biochemical modifications at the 5′ and 3′ ends of risiRNAs. The 5′ ends of risiRNAs were modified by phosphate groups, as risiRNAs cannot be labeled by T4 polynucleotide kinase (T4 PNK) without prior dephosphorylation treatment (**Supplementary Fig. 2b** and **Supplementary Data Set 2**). *In vitro* RNA capping reactions catalyzed by guanylyl transferase indicated that risiRNAs carry 5′ di- or triphosphates (**Supplementary Fig. 2c** and **Supplementary Data Set 2**). Guanylyl transferase can add a 7-methylguanylate (m^7G) to 5′ di- or triphosphate RNAs, which blocks downstream labeling of risiRNA. The presence of 5′ di- or triphosphates suggests that risiRNAs might be generated by RdRPs. The 3′ ends of risiRNAs contained a *cis*-diol, as shown by a β-elimination assay[14] (**Supplementary Fig. 2d** and **Supplementary Data Set 2**).

Genetic requirements of risiRNA generation

We searched for the genetic requirements of risiRNA biogenesis by setting up a quantitative TaqMan assay targeting a risiRNA sequence. SUSI-1, but not ERI-1, suppressed risiRNA production (**Fig. 3a**). ERI-1 is involved in 5.8S rRNA processing[22]. To exclude the possibility that ERI-1 is directly involved in 18S and 26S rRNA processing and the production of risiRNA, we generated *rrf-3(pk1426);susi-1(ust1);gfp::nrde-3* worms, in which the wild-type copy of *eri-1* is expressed. In *rrf-3(pk1426)* animals, NRDE-3 localized to the cytoplasm, whereas in the *susi-1(ust1)* mutant, NRDE-3 relocalized to the nucleus (**Fig. 3b**). The TaqMan assay confirmed the increase of risiRNA in *rrf-3(pk1426);susi-1(ust1)* animals (**Fig. 3c**). This result suggests that the *susi-1(ust1)* mutation is probably not a reversion of *eri-1(mg366)*.

The TaqMan assay showed that the nuclear RNAi factors NRDE-2 and NRDE-3 are not required for risiRNA accumulation (**Fig. 3d**). We analyzed previously published high-throughput deep sequencing data for *hrde-1(tm1200)* (ref. 23) and *mago12* (ref. 12) and found that HRDE-1 and other WAGO proteins may be required for the biogenesis and stability of risiRNA (**Supplementary Fig. 2e**). Notably, in the *prg-1(n4357)* strain[24], risiRNA is slightly increased, suggesting that certain 22G-RNA biogenesis factors may be shifted for risiRNA production when the piRNA-primed 22G-RNA synthesis pathway is disrupted[25,26]. However, it is unclear whether risiRNA can change the subcellular localization of PRG-1, HRDE-1 and other WAGO proteins.

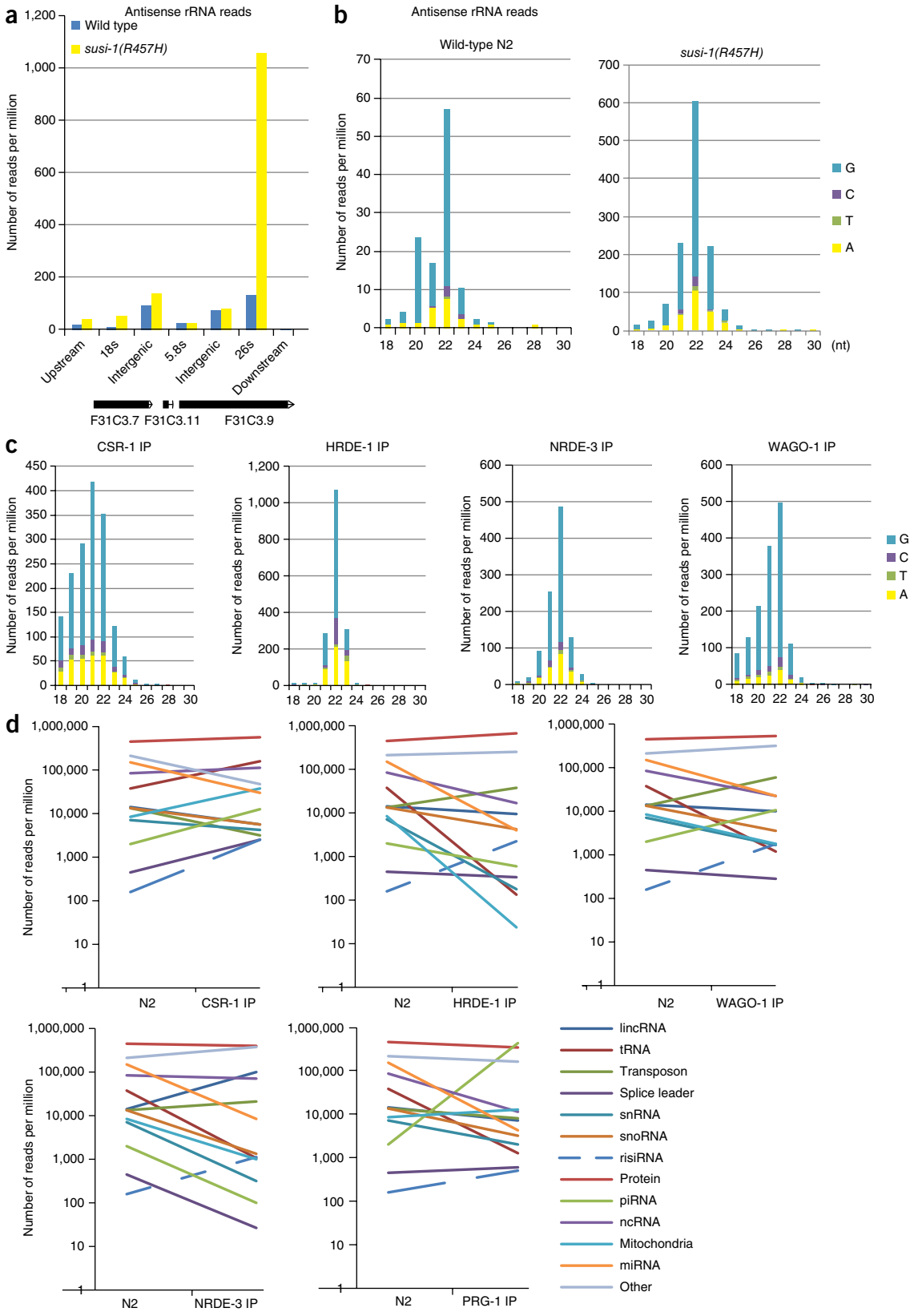

Figure 2 risiRNA belongs to the 22G-RNA class. (**a**) Deep sequencing of small RNAs in wild-type N2 and *susi-1*(*R457H*) mutant animals. The abundance of risiRNA is indicated. (**b**) Size distribution and 5′ end nucleotide preference of risiRNAs in wild-type N2 and *susi-1* (*R457H*) animals. (**c**) Size distribution and 5′ end nucleotide preference of risiRNAs identified in published data sets for Argonaute-associated small RNAs. IP, immunoprecipitate. (**d**) Relative abundance of Argonaute-associated small RNAs from published data sets.

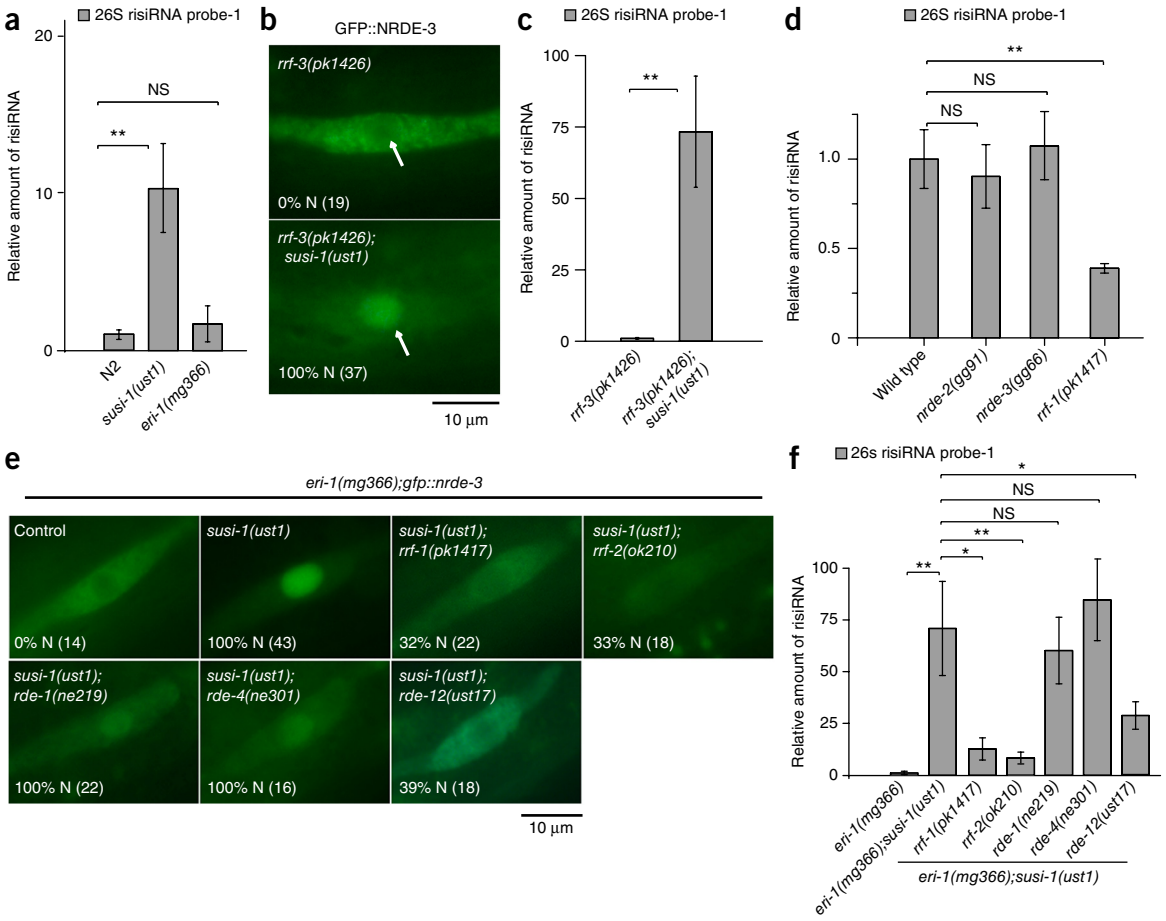

Figure 3 Genetic requirements for risiRNA biogenesis. (**a**) risiRNA abundance, quantified by TaqMan qRT-PCR from total RNA samples collected from bleached embryos of the indicated genotypes. Data are relative to levels in wild-type animals. (**b**) Images of GFP::NRDE-3 localization in seam cells of animals with the indicated genotype. The percentage of animals with nuclear-enriched NRDE-3 in seam cells is indicated (% N). The number of scored animals is indicated in parentheses. White arrows, nucleus. (**c**,**d**) Quantification of risiRNA as in **a**. (**e**) Seam cells of animals of the indicated genotypes expressing GFP::NRDE-3, labeled as in **b**. (**f**) Relative abundance of risiRNA, quantified as in **a**. Data are mean ± s.d. $n = 3$ animals; $^{*}P < 0.05$, $^{**}P < 0.01$, NS, not significant, two-tailed Student's *t*-test (**a**,**c**,**d**,**f**).

We crossed a number of existing mutants with the *eri-1(mg366);susi-1 (ust1);gfp::nrde-3* strain and found that *rrf-1*, *rrf-2* and *rde-12*, which are important for the generation of secondary endo-siRNAs, are required for risiRNA production. In worms in which these genes are mutated, NRDE-3 relocalized to the cytoplasm (**Fig. 3e**). These results were further confirmed by quantitative TaqMan assay (**Fig. 3f**).

The amount of risiRNA increased roughly ten-fold in the *susi-1* mutant (**Fig. 3a**). Notably, additional mutations in *eri-1* or *rrf-3* resulted in an ~75-fold upregulation of risiRNAs (**Fig. 3c**,**f**), suggesting that certain limiting factors, which are normally engaged in ERI–DICER-dependent endo-siRNA production, may have been used for the generation of risiRNAs in the *susi-1* mutant.

On the basis of the 5′ end nucleotide preference and modification, size distribution and genetic requirements, we concluded that risiRNA represents a novel class of regulatory 22G-RNAs whose generation depends on RdRP but not the ERI–DICER complex.

risiRNA silences expression of pre-rRNA

We tested whether risiRNA can silence rRNA. First, we generated a transgene expressing a *his-72*$_p$*::gfp::his-72* reporter fused to a 120-nt segment of the 26S rRNA sequence to make a risiRNA sensor (**Fig. 4a**). Whereas the control sensor is silenced by exogenous dsRNA targeting *gfp* but not the 26S rRNA, the risiRNA sensor can be silenced by feeding RNAi targeting either *gfp* or the 26S rRNA (**Supplementary Fig. 3a**). The sensor was expressed in wild-type N2 and *eri-1(mg366)* animals but silenced in *susi-1(ust1)* mutants (**Fig. 4b**), which was further confirmed by quantitative real-time PCR analysis (**Fig. 4c**).

In *susi-1(ust1)* animals, pre-rRNA was repressed, and mutations in *rrf-1* relieved the repression, as shown by quantitative real-time PCR analysis (**Fig. 4d–f**). Brood size was reduced in *eri-1(mg366);susi-1 (ust1)* mutants and partially restored by additional mutations in *rrf-1* or *rrf-2* (**Supplementary Fig. 3b**), suggesting that the silencing of pre-rRNA by risiRNA could be important for fertility in *C. elegans*.

Notably, the level of pre-rRNA suppression in each mutant did not correlate well with the level of risiRNA. The amounts of risiRNA decreased to similar levels with additional mutations in *rrf-1* or *rrf-2* (**Fig. 3f**), but derepression of rRNA was observed only in the *rrf-1* mutant (**Fig. 4f**). The difference in rRNA level resulted in similar restoration of brood size in *rrf-1* and *rrf-2* mutants (**Supplementary Fig. 3b**). It is possible that the level of pre-rRNA is modulated by both risiRNA-directed pre-rRNA silencing and the efficiency of SUSI-1-directed enzymatic degradation. SUSI-1(H654Y), a missense mutation, may exhibit different residual enzymatic capabilities in these mutant backgrounds. It is also possible that the pre-rRNA accumulated in an erroneous form in RdRP mutants or that SUSI-1 may have additional substrates besides rRNA that are important for fecundity.

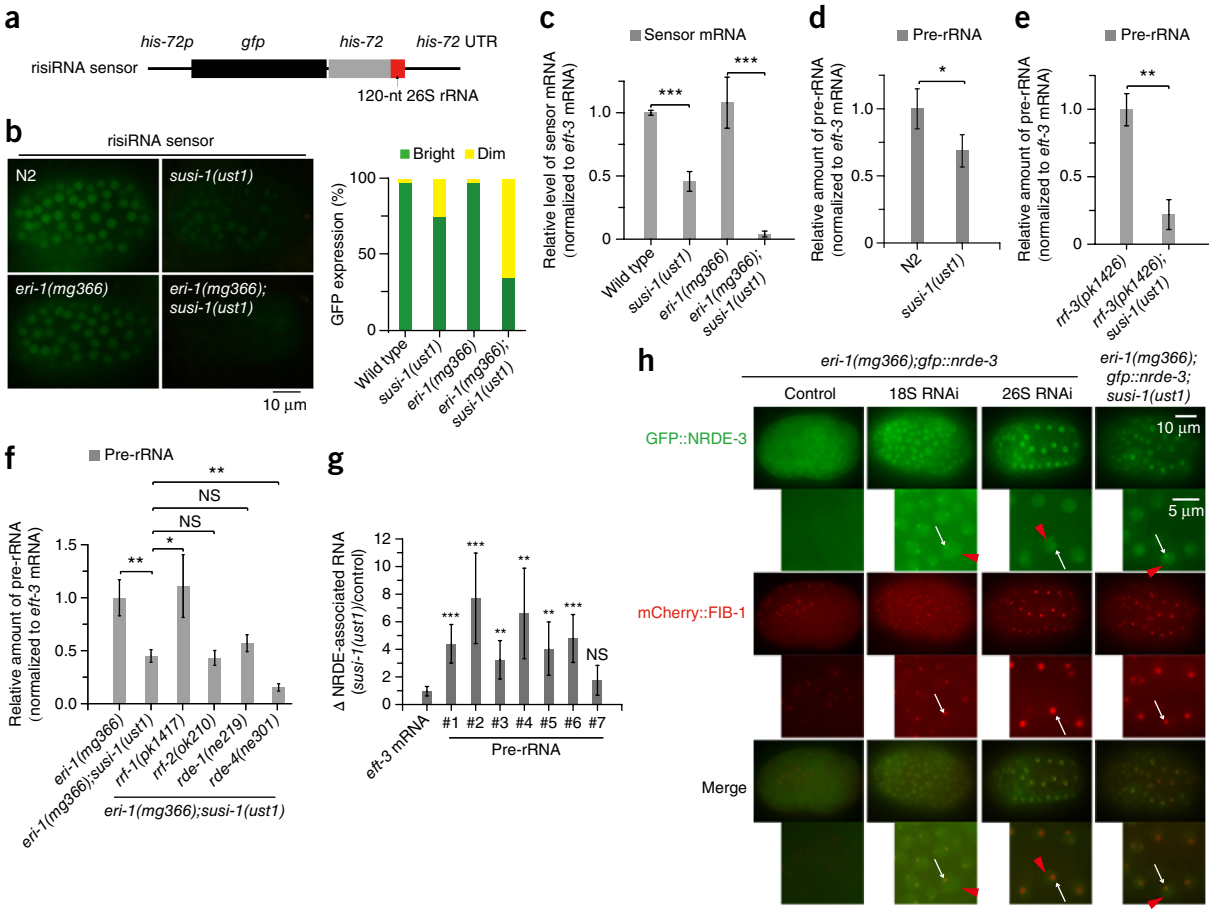

Figure 4 risiRNAs downregulate expression of pre-rRNA via the Nrde pathway. (**a**) Schematic representation of the risiRNA sensor. (**b**) Images of *C. elegans* embryos with the indicated genotypes expressing the risiRNA sensor at the ~300-cell stage. Right, quantification of GFP expression; ~20 embryos were scored for each genotype. (**c**) qRT-PCR analysis for risiRNA sensor mRNA on samples isolated from animals with the indicated genotypes. (**d**–**f**) qRT-PCR analysis for pre-rRNAs on RNA samples isolated from animals of the indicated genotypes (**g**) Abundance of pre-rRNA associated to NRDE-3, quantified by qRT-PCR and shown relative to levels of co-precipitated *eft-3* mRNA. Primer pairs are described in **Supplementary Figure 3c**. (**h**) Images of *C. elegans* embryos with the indicated genotypes expressing GFP::NRDE-3 at the ~300-cell stage. Magnified images are shown below each image. Red triangle, nucleus; white arrows, nucleoli. Data are mean ± s.d. $n = 3$ animals; $^*P < 0.05$, $^{**}P < 0.01$, $^{***}P < 0.001$, NS, not significant, two-tailed tailed Student's *t*-test (**c**–**g**).

risiRNA silences pre-rRNA via the nuclear RNAi pathway

Three lines of evidence cumulatively supported the idea that risiRNA can act via the nuclear RNAi pathway. First, we immunoprecipitated NRDE-3 and quantified its associated RNA by real-time PCR. Feeding RNAi targeting 18S or 26S rRNA elicited the binding of NRDE-3 to pre-rRNAs (**Supplementary Fig. 3c**). NRDE-3(*PAZ), which contains a mutation in the PAZ domain of NRDE-3 and disrupts its ability to bind siRNA[14], failed to bind to targeted pre-rRNAs. Second, NRDE-3 also associated with pre-rRNA in the *susi-1(ust1)* mutant (**Fig. 4g**).

Third, we observed nucleolar accumulation of NRDE-3 after exogenous RNAi targeting 18S and 26S rRNAs as well as in *susi-1(ust1)* animals (**Fig. 4h**). FIB-1 in *C. elegans* is encoded by an ortholog of the genes encoding human fibrillarin and *Saccharomyces cerevisiae* Nop1p[27,28]. FIB-1 localizes to the nucleolus in embryos. Feeding *eri-1(mg366);gfp::nrde-3* animals with exogenous dsRNA targeting 18S and 26S rRNAs elicited nucleolar accumulation of NRDE-3, which colocalized with FIB-1. Consistently, NRDE-3 localized to nucleoli in *eri-1(mg366);susi-1(ust1);gfp::nrde-3* animals as well.

Therefore, risiRNA appears to act, at least in part, through the Nrde pathway to regulate pre-rRNA expression.

Temperature affects risiRNA and pre-rRNA via the Nrde pathway

We wondered whether risiRNA has regulatory functions at physiological conditions in wild-type animals. We noticed a dramatic decrease of brood size of *eri-1(mg366);susi-1(ust1)* at 15 °C (**Supplementary Fig. 4a**), suggesting that risiRNAs may be responsive to temperature alterations. Therefore, we examined the expression of risiRNA and pre-rRNA at different temperatures (**Fig. 5a**).

We found that both risiRNA sensor mRNA and GFP intensity decreased with temperature reduction in the wild-type N2 and *eri-1* backgrounds (**Fig. 5b**,**c**). Lower temperature increased the expression of risiRNA in both N2 and *nrde-2(gg98)* animals at 4 °C and 15 °C (**Fig. 5d**). Consistently, the expression of pre-rRNA was downregulated at lower temperatures in N2 animals but not in *nrde-2* mutants (**Fig. 5e**), suggesting that low temperatures suppress pre-rRNA via risiRNA and the Nrde pathway even in the *susi-1*$^{+/+}$ background. But this temperature-dependent generation of risiRNAs was more pronounced in the *susi-1(ust1)* mutant (**Supplementary Fig. 4b**). Notably, the upregulation of risiRNA at lower temperatures was more dramatic in *eri-1(mg366)* than in N2 animals (**Fig. 5d**), which is consistent with the prediction that risiRNAs compete for the same limiting factors for ERI–DICER-dependent generation of 22G-RNA. We also found

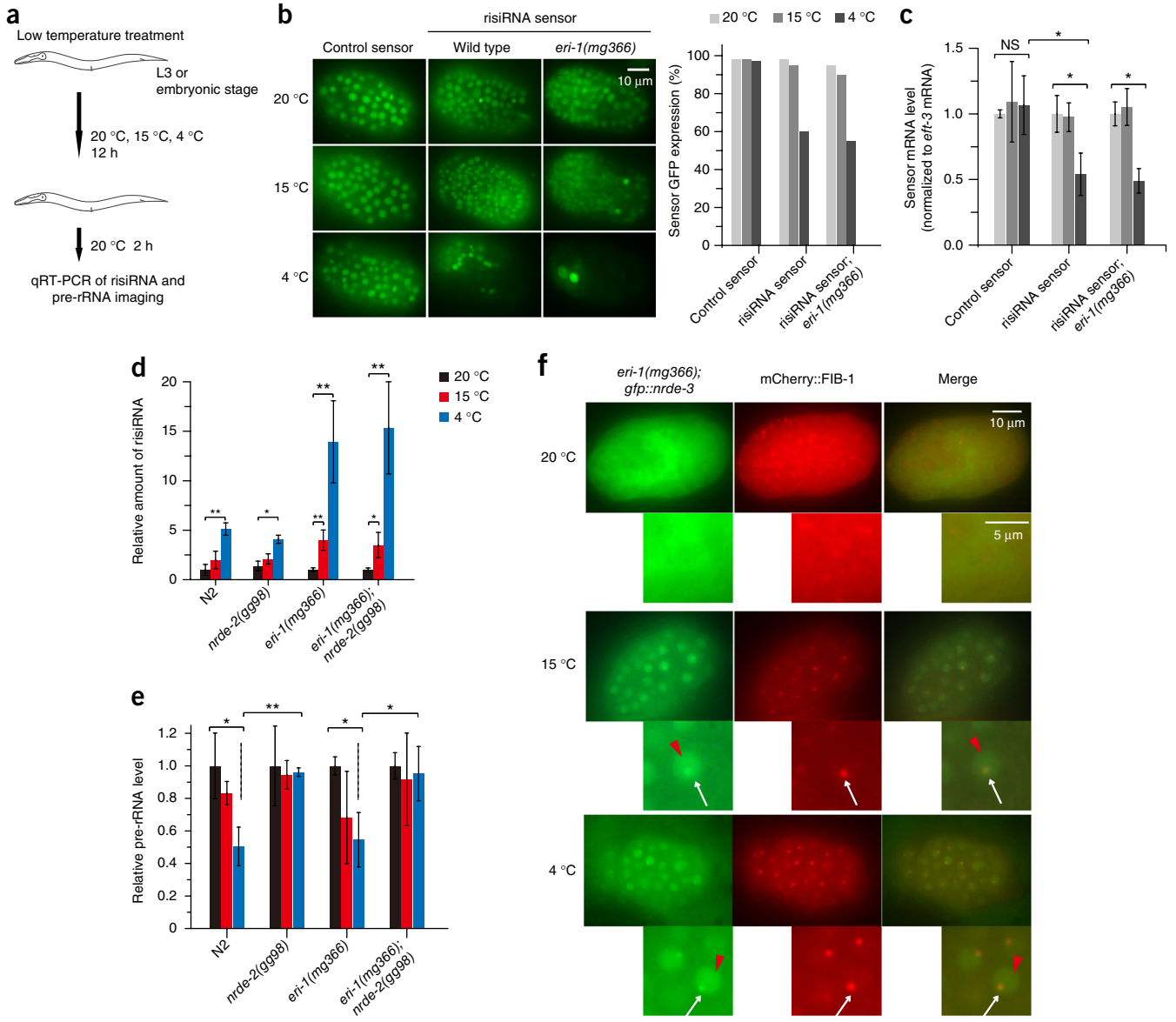

Figure 5 Lowering temperature increased expression of risiRNA. (**a**) Schematic of the low-temperature treatment assay. (**b**) Images (left) and scoring (right) of embryos expressing the risiRNA sensor at the ~300-cell stage. (**c**) Abundance of risiRNA sensor mRNA in total RNA samples collected from bleached embryos, quantified by qRT-PCR and shown relative to levels at 20 °C. (**d**) Abundance of risiRNA in total RNA samples collected from bleached embryos of the indicated genotypes, quantified by TaqMan qRT-PCR and shown relative to levels at 20 °C. (**e**) Abundance of pre-rRNA quantified by qRT-PCR in samples as in **d**. (**f**) Images of *C. elegans* embryos with the indicated genotypes expressing GFP::NRDE-3 at the ~300-cell stage. Red triangle, nucleus; white arrows, nucleoli. Data are mean ± s.d. $n = 3$ animals; $^*P < 0.05$, NS, not significant. two-tailed Student's *t*-test (**c**–**e**).

that the temperature-dependent generation of risiRNAs still relies on RdRPs, including RRF-1 and RRF-2 (**Supplementary Fig. 4c**).

We investigated whether low temperature can cause relocalization of NRDE-3 to the nucleus and nucleoli. NRDE-3 is found mainly in the cytoplasm in *eri-1(mg366);gfp::nrde-3* animals at 20 °C. Shifting the temperature to 4 °C and 15 °C relocalized NRDE-3 to the nucleus in larvae and the nucleoli in embryos (**Fig. 5f** and **Supplementary Fig 4d**). NRDE-3(*PAZ) did not respond to temperature alterations. *rrf-1* and *rde-12* were required for this temperature-dependent cytoplasm-to-nucleus translocation of NRDE-3 (**Supplementary Fig. 4d**).

We deep sequenced small RNAs from wild-type N2 *C. elegans* after cold shock at 4 °C for 12 h at the embryonic stage and a 2-h recovery (**Fig. 5a**). Total RNA was isolated and subjected to high-throughput sequencing. The number of risiRNA reads increased ~3.4-fold (556 reads per million in cold-shocked N2 animals versus 162 reads per million at 20 °C) (**Supplementary Fig. 5a**). We cold shocked *gfp::nrde-3* embryos, immunoprecipitated NRDE-3 and deep sequenced NRDE-3-associated small RNAs. risiRNA was enriched ~8.8-fold (10,006 reads per million in cold-shocked *gfp::nrde-3* animals versus 1,134 reads per million at 20 °C) (**Supplementary Fig. 5b**). We then cold shocked *eri-1(mg366);gfp::nrde-3* and deep sequenced NRDE-3-associated small RNAs. Because NRDE-3 binds very few endo-siRNAs at 20 °C in *eri-1* animals[14], we reanalyzed published data from small RNA deep sequencing of NRDE-3 immunoprecipitation in *eri-1 (mg366);dpy-13(e458);dpy-13(RNAi);gfp::nrde-3* animals[18]. Feeding

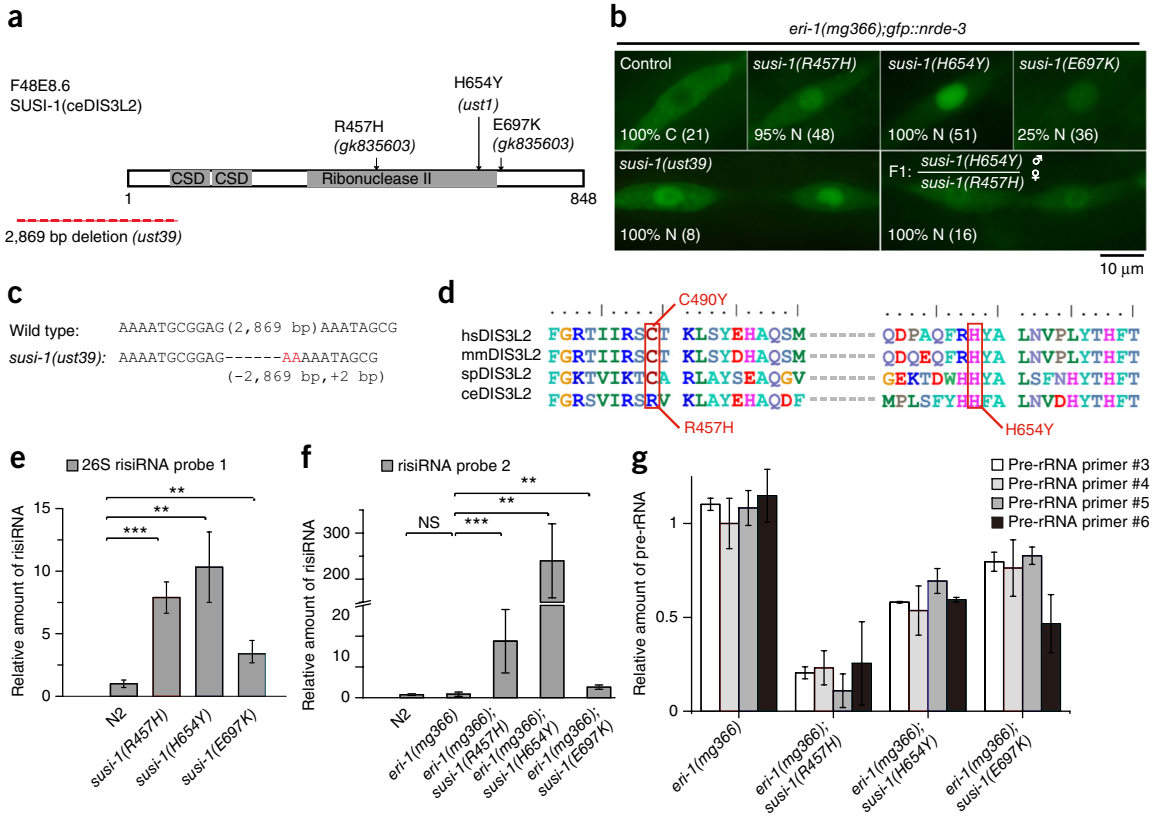

Figure 6 SUSI-1(ceDIS3L2) suppresses risiRNA accumulation. (**a**) Schematic of SUSI-1(ceDIS3L2) and the four mutant alleles in which NRDE-3 accumulated in the nucleus. CSD, cold sensitive domain. (**b**) Images of seam cells of GFP::NRDE-3-expressing *C. elegans* with the indicated genotypes. The percentages of animals showing at least one seam cell with nuclear-enriched NRDE-3 is indicated (% N). The numbers of scored animals are indicated in parentheses. C, cytoplasmic localization. (**c**) Sequence alignment of the *susi-1*(*ust39*) allele generated by CRISPR–Cas9-directed gene deletion. (**d**) Sequence alignments of DIS3L2 in different organisms. hs, homo sapiens; mm, *Mus musculus*; sp, *Schizosaccharomyces pombe*; ce, *C. elegans*. (**e**,**f**) Abundance of risiRNA in total RNA samples collected from bleached embryos of the indicated genotypes, quantified by TaqMan qRT-PCR and shown relative to levels in wild-type animals. (**g**) Abundance of pre-rRNA quantified by qRT-PCR in samples as in **e**. The real-time PCR primers for pre-rRNA detection are described in **Supplementary Figure 3c**. Data are mean ± s.d. $n = 3$ animals; $^{*}P < 0.05$, $^{**}P < 0.01$, $^{***}P < 0.001$, NS, not significant, two-tailed Student's *t*-test (**e**–**g**).

exogenous dsRNA targeting the gene *dpy-13* elicited nuclear accumulation of NRDE-3 in the *eri-1* mutant background. Notably, risiRNA was enriched to approximately 226 fold (1,669 reads in *eri-1(mg366); dpy-13(e458);dpy-13(RNAi);gfp::nrde-3* versus 377,532 reads in cold-shocked *eri-1(mg366);gfp::nrde-3*) (**Supplementary Fig. 5c**).

SUSI-1 is a homolog of human DIS3L2

We mapped *susi-1(ust1)* to a <0.2-cM interval, deep sequenced the *susi-1(ust1)* genome and identified F48E8.6, an open reading frame (ORF) that contains a T-to-C mutation encoding an H654Y substitution (**Fig. 6a**). Alleles encoding R457H and E697K substitutions in SUSI-1 (ref. 29) also induced redistribution of NRDE-3 to the nucleus (**Fig. 6b** and **Supplementary Table 3**). The two alleles were generated in the *C. elegans* Million Mutation Project[29] by ethyl methanesulfonate–induced random mutagenesis without phenotypic selection. Most alleles generated by this method do not change the function of a desired gene. Consistently, most *susi-1* alleles failed to relocalize NRDE-3 to the nucleus (**Supplementary Table 3**).

To further confirm that F48E8.6 is *susi-1*, we generated a large deletion allele of F48E8.6 by CRISPR–Cas9 technology with two single guide RNAs (sgRNAs)[30] (**Fig. 6c**). This mutation, termed *susi-1(ust39)*, removed 2,107 nt of the promoter region and the first 256 codons and is likely to be a null allele. NRDE-3 accumulated in the nucleus in *eri-1(mg366);susi-1(ust39);gfp::nrde-3* animals (**Fig. 6b**). Moreover, injection of an mCherry::F48E8.6 expression plasmid into *eri-1(mg366);susi-1(ust1);gfp::nrde-3* animals relocated NRDE-3 to the cytoplasm (**Supplementary Fig. 6a**). Therefore, F48E8.6 is *susi-1*. Because *susi-1(ust1)* was the first allele identified from our forward genetic screen, it was outcrossed five times and used as the reference allele.

SUSI-1 is a conserved protein that shows extensive homology to human DIS3L2, which is linked to Perlman syndrome, Wilm's tumor development, early embryogenesis and stem cell proliferation[31,32]. DIS3L2 contains a RNase II domain and functions in the RNA surveillance pathway[33–36]. *susi-1(ust1, H654Y)* encodes a change in the conserved amino acid in the RNase domain (**Fig. 6d**). Notably, *susi-1 (gk835603)* contains the mutation encoding R457H, which was discovered at the same position in patients with Perlman syndrome. In *susi-1(R457H)* and *susi-1(E697K)* animals, risiRNAs accumulated and pre-rRNAs were downregulated (**Fig. 6e–g**). These observations confirmed that SUSI-1(ceDIS3L2) is involved in the regulation of risiRNA and pre-rRNA.

As observed above, the levels of pre-rRNA suppression in each mutant did not correlate very well with the levels of risiRNA (**Fig. 6e–g**). One possible explanation is that the level of pre-rRNA is modulated by both risiRNA-directed pre-rRNA silencing and the

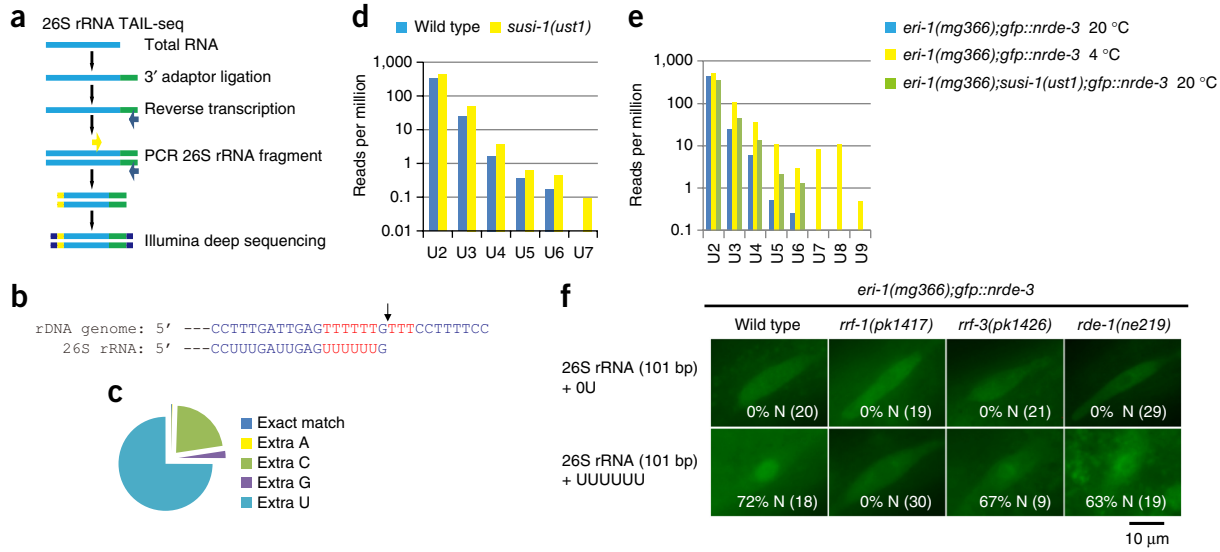

Figure 7 Oligouridylated 26S rRNA promotes risiRNA generation. (**a**) Schematic of 26S rRNA TAIL-seq method. (**b**) Sequence alignment of rDNA and 26S rRNA from the WormBase WS250 assembly. (**c**) TAIL-seq of 26S rRNA from wild-type N2 animals. The amount of 3′-end untemplated addition of single nucleotides is indicated. (**d**,**e**) TAIL-seq of 26S rRNA from indicated animals. The 3′-end untemplated oligouridylation is indicated. (**f**) Injection of 3′-tail-oligouridylated 26S rRNA fragments into animals with the indicated genotypes expressing GFP::NRDE-3. The percentage of animals that exhibit at least one seam cell with nuclear-enriched NRDE-3 is indicated (N %). The number of injected animals are indicated in parentheses.

efficiency of SUSI-1(ceDIS3L2)-directed enzymatic degradation. The R457H and H654Y missense mutations may exhibit different enzymatic capabilities to degrade erroneous pre-rRNA.

We generated GFP-fused *susi-1(ceDIS3L2)* transgenic lines and found that SUSI-1(ceDIS3L2) mainly localized in the cytoplasm (**Supplementary Fig. 6b**). *susi-1* mutants displayed decreased brood size and embryogenesis defects (**Supplementary Fig. 6c**,**d**), suggesting that SUSI-1(ceDIS3L2) has important roles in the development of *C. elegans*.

SUSI-1(ceDIS3L2) is involved in oligouridylated rRNA degradation

DIS3L2 is a 3′–5′ exoribonuclease that acts preferentially on oligo (U)-tailed transcripts, yet its endogenous substrates remain unclear. We used a 3′ TAIL-seq assay to examine whether 3′-tail-oligouridylated rRNA accumulated in *susi-1(ust1)* (**Fig. 7a**). Total RNAs were ligated to a barcoded DNA linker and reverse transcribed with a primer complementary to the linker. Libraries were then prepared by PCR with a 26S rRNA primer and a primer targeting the linker. Illumina adaptor sequences were then added for PCR and high-throughput sequencing.

Notably, the 3′ end of 26S rRNA was extensively modified by all four nucleotides, when compared to the annotated rRNA sequence (**Fig. 7b**,**c**). Only a small fraction of the 3′ ends matched the annotated 26S rRNA from the WormBase WS250 assembly exactly. The extra U matched the genomic sequence (we consider this extra U as an addition rather than a promiscuous rRNA termination, because a substantial fraction of the 26S rRNAs were ended with nontemplated A, C and G). Although we did not detect a dramatic change of the nontemplated addition of single nucleotide (**Supplementary Fig. 7a**,**b**), we observed a modest increase of 3′-tail-oligouridylated 26S rRNA in *susi-1(ust1)* compared to wild-type N2 (**Fig. 7d**) and in *eri-1(mg366);susi-1(ust1);gfp::nrde-3* animals compared to *eri-1(mg366); gfp::nrde-3* (**Fig. 7e**). In addition, *eri-1(mg366); gfp::nrde-3* also increased untemplated oligouridylation in response to a decrease in temperature, to 4 °C (**Fig. 7e**).

To further demonstrate that 3′-tail-oligouridylated 26S rRNA triggered risiRNA production, we injected 26S rRNA fragments with or without a UUUUUU 3′ tail into *eri-1(mg366); gfp::nrde-3* at the L3/L4 larval stage. The subcellular localization of *gfp::nrde-3* was monitored after 2 h. The 3′ tail oligouridylation of 26S rRNA stimulated the nuclear accumulation of NRDE-3 (**Fig. 7f**). This cytoplasm-to-nucleus translocation of NRDE-3 was suppressed in *rrf-1* but not in *rrf-3* or *rde-1* mutants.

Therefore, we conclude that oligouridylated rRNAs accumulate in *susi-1* mutants, which promote the generation of risiRNA and the relocalization of NRDE-3.

Effect of UV irradiation on NRDE-3 and risiRNA expression

We tested whether other kinds of stress besides cold shock can lead to the accumulation of risiRNAs and observed that UV irradiation triggers the cytoplasm-to-nucleus translocation of NRDE-3 and enhances risiRNA expression.

Upon UV irradiation, NRDE-3 translocated to the nucleus in L3/L4 animals as well as in embryos in *eri-1(mg366);gfp::nrde-3* animals (**Fig. 8a**,**b**). NRDE-3(PAZ*) did not accumulate in the nucleus after UV exposure, suggesting that the UV-induced NRDE-3 translocation depends on its ability to bind small RNAs. NRDE-3 accumulated in nearly all of the embryos in 2 h after UV exposure (**Supplementary Fig. 8a**). Notably, UV irradiation did not trigger a pronounced nucleolar accumulation of NRDE-3 (**Supplementary Fig. 8b**). We observed disassembly of the mCherry::FIB-1 foci in the nucleus, suggesting that the nucleoli may have been disorganized upon UV exposure.

We immunoprecipitated NRDE-3 and labeled its bound RNA with ^{32}P. Upon UV exposure, NRDE-3 became reassociated with 20–22-nt small RNAs in *eri-1(mg366);gfp::nrde-3* animals (**Fig. 8c** and **Supplementary Data Set 3**). We deep sequenced NRDE-3-associated small RNAs from UV-treated *eri-1(mg366);gfp::nrde-3* animals and identified risiRNA as well (**Fig. 8d**). risiRNA was enriched ~16-fold in immunoprecipitated samples (1,669 reads per million without

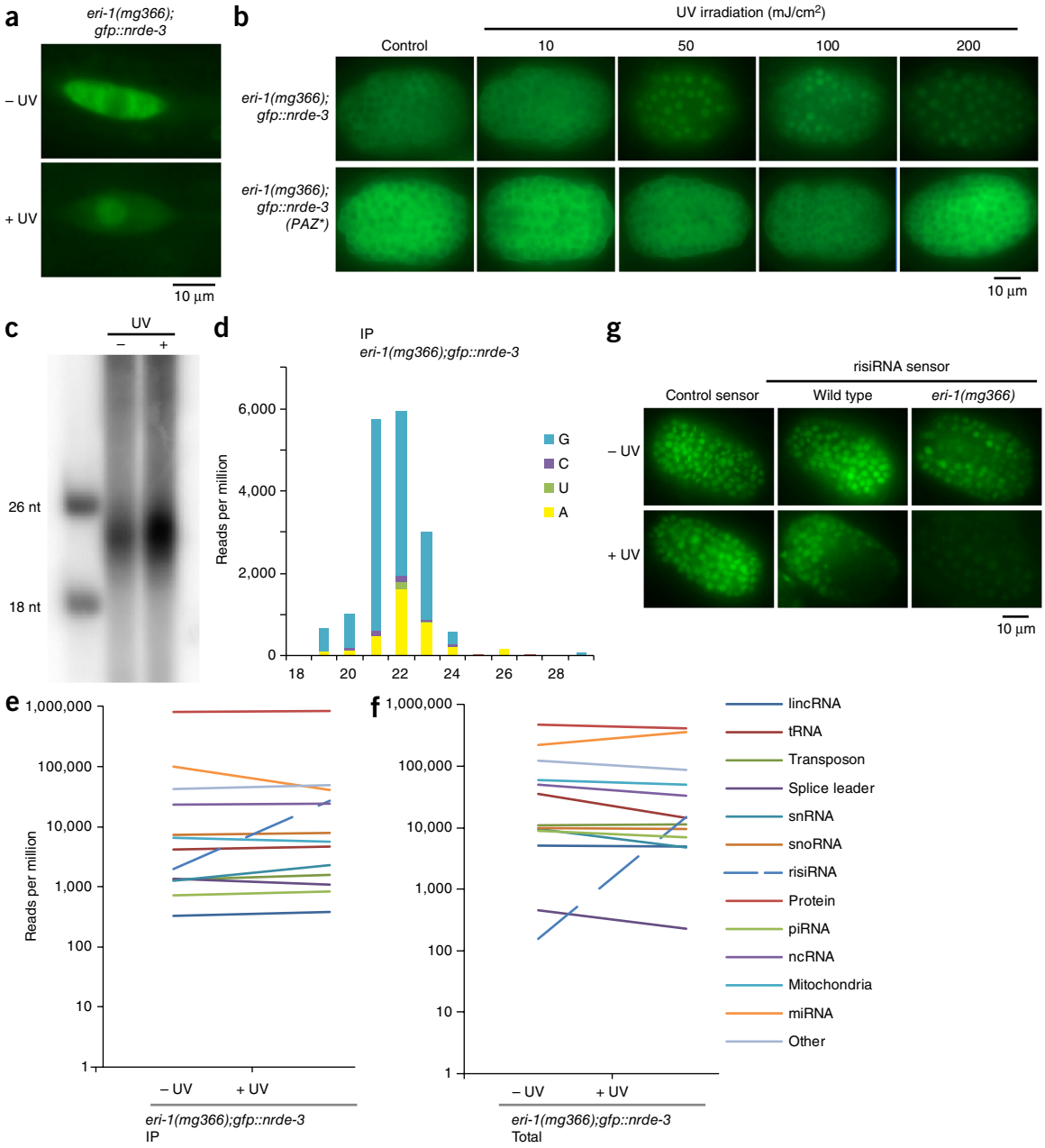

Figure 8 UV irradiation enhances risiRNA accumulation and triggers redistribution of NRDE-3 to the nucleus. (**a**) Subcellular localization of GFP::NRDE-3 in seam cells, visualized in L3 animals 2 h after exposure to 50 mJ/cm^2 UV irradiation. (**b**) Subcellular localization of GFP::NRDE-3 in bleached embryos 2 h after exposure to different doses of UV irradiation. (**c**) NRDE-3-associated small RNAs of the indicated animals were immunoprecipitated, labeled with ^{32}P and resolved by gel electrophoresis. An uncropped gel image is shown in **Supplementary Data Set 3**. (**d**–**f**) Deep sequencing of small RNAs in *eri-1(mg366);gfp::nrde-3* animals after UV exposure. (**d**) Antisense rRNA reads from NRDE-3 immunoprecipitation (IP). Size distribution and 5′-end nucleotide preference of risiRNAs are indicated. (**e**) Relative abundance of NRDE-3-associated small RNAs. The blue dashed line indicates risiRNAs. (**f**) Relative abundance of total small RNAs. (**g**) Images of *C. elegans* embryos expressing the risiRNA sensor after UV exposure at the ~300-cell stage.

UV treatment and 26,688 reads per million with UV treatment in *eri-1(mg366);gfp::nrde-3*) (**Fig. 8e**). For total small RNAs from bleached embryos with or without UV exposure, the number of risiRNA reads was increased ~99-fold (153 reads per million in untreated versus 15,079 reads per million in UV-treated *eri-1(mg366);gfp::nrde-3*) (**Fig. 8f**). The enrichment of risiRNA was confirmed by quantitative real-time PCR (**Supplementary Fig. 8c**,**d**). Furthermore, UV exposure silenced the risiRNA sensor but not the control sensor, which lacks the risiRNA-targeted sequences (**Fig. 8g**).

Therefore, both cold shock and UV irradiation stimulate risiRNA expression, suggesting that risiRNA may act as a buffer against various stress conditions.

DISCUSSION

The biogenesis of small RNAs is highly regulated during development and disease and in response to environmental stimuli. Here we describe a novel class of risiRNAs that exhibit characteristics of 22G-RNA. risiRNAs regulate pre-rRNA expression, at least in part,

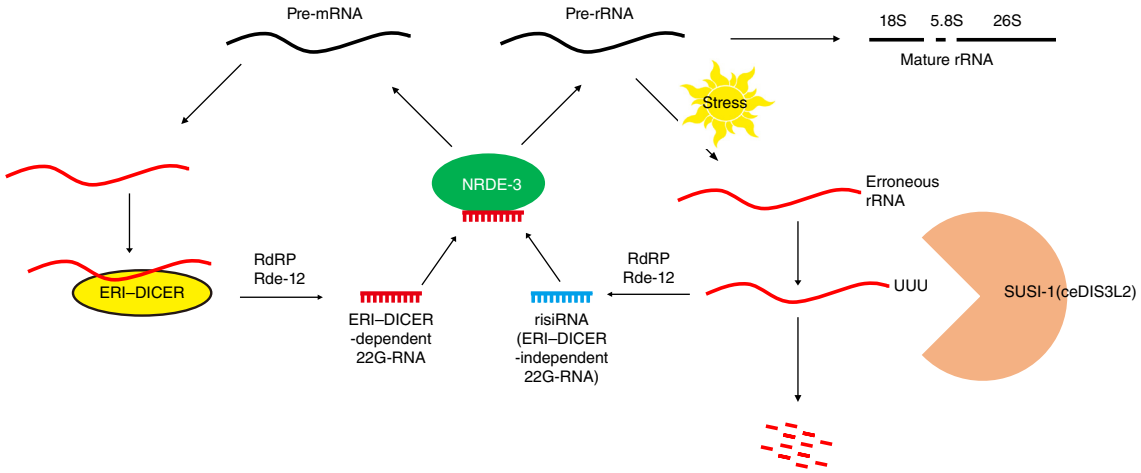

Figure 9 A working model for risiRNA- and NRDE-mediated pre-rRNA regulation. Erroneous rRNAs are modified by polyuridylation and degraded by exonucleases, such as SUSI-1(ceDIS3L2). The dysfunction of these exonucleases results in the accumulation of erroneous rRNAs, which recruit RdRP to synthesize risiRNA. NRDE-3 binds both ERI–DICER-dependent 22G-RNA and ERI–DICER-independent risiRNA to silence their respective targets. Therefore, the NRDE-mediated feedback loop may compensate for dysfunction of exonuclease-directed degradation of erroneous rRNA transcripts. Knocking out the ERI–DICER complex will disrupt normal biogenesis of 22G-RNA and redistribute RdRPs for production of risiRNA and NRDE-3 for silencing of pre-rRNA.

through the nuclear RNAi pathway, therefore providing a new layer of regulatory strategy in rRNA homeostasis and translational control. We also found that SUSI-1(ceDIS3L2) is involved in suppressing risiRNA accumulation. In the *susi-1*(*ceDIS3L2*) mutant, 3′-tail-oligouridylated 26S rRNA fragments were enriched.

risiRNAs are widely present in various organisms

Small rRNAs have long been viewed as degradation products and are usually discarded during high-throughput RNA-seq analyses. Here we showed that risiRNAs have characteristics of 22G-RNA, both biochemically and genetically. Unlike other subset of 22G-RNAs, the biogenesis of risiRNA is independent of the ERI–DICER complex and is normally suppressed but upregulated by various stress stimuli. In addition, risiRNAs utilize 3′-tail-polyuridylated rRNA rather than mRNA as a template. Taken together with their ability to bind NRDE-3, these results indicate that risiRNAs could have important physiological functions.

Antisense rRNAs are widely present in various organisms. In *Schizosaccharomyces pombe* lacking Cid14, rRNAs become substrates for the RNAi pathway and give rise to siRNAs targeting rRNA[37]. In *Neurospora crassa*, DNA damage induces the expression of the Argonaute protein QDE-2 and a class of RNAs that interact with it (qiRNAs) from the ribosomal DNA locus[38]. The activation of antiviral RNAi in *Arabidopsis* induces the production of risiRNAs as well[39].

risiRNAs downregulate rRNA expression

The biogenesis of rRNA drives cell growth and proliferation, but mechanisms that modulate rRNA production and processing remain poorly understood[40]. Noncoding RNAs are involved in rRNA processing and maturation, in which small nucleolar RNAs (snoRNAs) are well known to have central roles. Other nucleolar noncoding RNAs have also been identified to function in pre-rRNA processing[41].

Here we showed that risiRNAs suppress rRNA at least in part through the nuclear RNAi pathway. Small RNA has been shown to recruit the NRDE complex to targeted nascent transcripts, induce H3K9 and H3K27 trimethylation, pause RNA polymerase II and induce premature termination of transcription[42–44]. It will be interesting to test whether risiRNAs modulate rRNA transcription via similar mechanisms.

Oligouridylated rRNA fragments promote 22G-RNA production

RNA molecules are subjected to post-transcriptional modifications that can determine their maturation, activity, localization and stability. One type of modification is the 3′-end addition of nontemplated nucleotides. Although polyadenylation is usually thought to stabilize mRNA, oligouridylation is required for 3′–5′ degradation of histone mRNAs[45,46]. In *C. elegans*, RDE-3 probably uridylates 5′ fragments of the targeted mRNA, a process required for the amplification of secondary siRNA[5].

We found that oligouridylated rRNA accumulated in the *susi-1 (ceDIS3L2)* mutant. Therefore, SUSI-1(ceDIS3L2) may act as an rRNA surveillance factor to degrade oligouridylated rRNA, which may arise from erroneous rRNA processing or modifications (**Fig. 9**). The RNAi pathway may assist SUSI-1(ceDIS3L2) in RNA surveillance. Whereas oligouridylated rRNA accumulates because of the dysfunction of SUSI-1(ceDIS3L2), RdRPs will be recruited to these erroneous rRNAs and generate risiRNAs to downregulate rRNA transcripts.

We did not see *susi-1*-dependent generation of risiRNA targeting 5S RNA. Eukaryotic 5S rRNA is synthesized by RNA polymerase III, whereas other eukaryotic rRNAs are cleaved from a 45S precursor transcribed by RNA polymerase I. Whether SUSI-1(ceDIS3L2) is able to act on erroneous 5S rRNA requires further investigation.

DIS3L2, oligouridylated rRNA and disease

DIS3L2 is a 3′–5′ exoribonuclease from the RNase II/RNB family that acts preferentially on oligo(U)-tailed transcripts[33–36]. Human DIS3L2 has been linked to Perlman syndrome and other diseases[31,32]. However, the endogenous substrates of DIS3L2 remain mysterious. Here we showed that oligouridylated rRNA accumulated in the *susi-1(ceDIS3L2)* mutant, suggesting that DIS3L2 may regulate rRNA biogenesis. However, the physiological outcomes of risiRNA and these erroneous rRNAs need further investigation.

SUSI-1(ceDIS3L2) is probably required for the accumulation of some endogenous small regulatory RNAs, including piRNA and microRNA. Recent work also showed that DIS3L2 regulates both RNA polymerase II (Pol II) and Pol III transcripts[47]. Together with our result of the Pol I–transcribed rRNA, we conclude that DIS3L2 can have critical roles in maintaining transcriptome homeostasis.

Stress-regulated rRNA biogenesis

Temperature has profound effects on rRNA biogenesis and processing, assembly of ribonucleoprotein particles and genome integrity of ribosomal DNA[48–53]. Here we showed that lower temperature could impair 3′-end maturation of 26S rRNA, trigger risiRNA expression and downregulate pre-rRNA. Analyzing the enzymatic activities of SUSI-1(ceDIS3L2) and other RNA processing and surveillance factors will help to elucidate the temperature-dependent generation of oligouridylated rRNA and risiRNA.

We also observed that UV irradiation triggers the cytoplasm-to-nucleus translocation of NRDE-3 and specifically increases risiRNA expression. UV exposure has profound effects on cellular macromolecules, including induction of intra- and inter- molecular cross-linking. These erroneous nucleic acids, including rRNAs, may recruit RdRPs and trigger *de novo* synthesis of secondary siRNAs. We speculate on the basis of these results that risiRNAs may act to buffer against many kinds of stress conditions to maintain the homeostasis of cellular rRNA levels.

risiRNA and 22G-RNA compete for the nuclear RNAi pathway

Several lines of evidence cumulatively suggest that risiRNAs reflect errors in the template for small RNA biogenesis, but not in the small RNA production machinery. First, SUSI-1(ceDIS3L2) is an exonuclease targeting polyuridylated rRNA. In the *susi-1* mutant, the small RNA generation machineries are intact. Second, the injection of polyuridylated rRNA triggers the generation of risiRNAs. Third, stress stimuli substantially upregulate risiRNA but not other classes of small RNAs.

ERI–DICER is required for the production of endogenous 22G-RNA[54]. Here we showed that risiRNAs mostly target 18S and 28S rRNAs and that the biogenesis of risiRNA is independent of the ERI–DICER complex. NRDE-2 regulates the expression of pre-rRNA at different temperatures, further supporting that ERI-1 is not directly involved in risiRNA biogenesis. Therefore, we speculate that mutations in the ERI–DICER complex disable the normal biogenesis machinery for endogenous 22G-RNA and redistribute RdRPs for the generation of risiRNA. Both risiRNA and ERI–DICER-dependent 22G-RNA engage the Nrde pathway to silence their respective targets in the nucleus (**Fig. 9**). Further experiments are required to examine how erroneous rRNAs are produced and recruited to the RNAi machinery. It will also be interesting to test whether risiRNAs silence pre-rRNA via prohibition of RNA Pol I–mediated transcription elongation.

risiRNA may engage many WAGO-mediated silencing pathways

22G-RNAs function mainly via binding to distinct WAGOs and eliciting different gene silencing mechanisms to negatively regulate their respective targets. We detected the association of risiRNAs with multiple WAGO proteins, suggesting that risiRNA may silence rRNAs via multiple mechanisms, including but not limited to the NRDE-3-engaged nuclear RNAi pathway, to maintain the homeostasis of rRNA and translation. This flexibility may help *C. elegans* to quickly and efficiently respond to environmental alterations and facilitate survival in stress conditions. Further investigation of the association of risiRNAs to these Argonaute proteins under various stress conditions or in *susi* mutants would help to pinpoint the functional significance and mechanisms of risiRNA.

METHODS

Methods, including statements of data availability and any associated accession codes and references, are available in the online version of the paper.

Note: Any Supplementary Information and Source Data files are available in the online version of the paper.

ACKNOWLEDGMENTS

We are grateful to S. Kenney, X. Fu, B. Buckley, X. Liu, B. Dong, C. Liu and members of S.G.'s lab for their comments. We are grateful to the Caenorhabditis Genetics Center (CGC), the International *C. elegans* Gene Knockout Consortium and the National Bioresource Project for providing the strains. A. Fire (Stanford University) provided HT115 bacteria expressing the empty vector L4440. This work was supported by grants from the National Natural Science Foundation of China (31371323, 31671346, 91640110 and 81501329), the Fundamental Research Funds for Central Universities (WK2060190018 and WK2070000034) and KJZD-EW-L01-2 to S.G.

AUTHOR CONTRIBUTIONS

X.Z. constructed the transgenes and generated **Figures 3**–**7**, **Supplementary Figures 3**, **4** and **6** and **Supplementary Tables 1** and **3**. X.F. conducted the genetic screening, identified risiRNA, mapped susi-1 and contributed to **Figures 1**, **2** and **8**, **Supplementary Figures 2**, **5**, **7** and **8** and **Supplementary Table 2**. H.M. contributed to **Figure 8** and **Supplementary Figure 8**. M.L., F.X. and K.H. contributed to **Figure 3b**,**e**. X.Z., X.F. and S.G. designed the project and wrote the manuscript.

COMPETING FINANCIAL INTERESTS

The authors declare no competing financial interests.

1. Czech, B. & Hannon, G.J. Small RNA sorting: matchmaking for Argonautes. *Nat. Rev. Genet.* **12**, 19–31 (2011).
2. Siomi, H. & Siomi, M.C. On the road to reading the RNA-interference code. *Nature* **457**, 396–404 (2009).
3. Ghildiyal, M. & Zamore, P.D. Small silencing RNAs: an expanding universe. *Nat. Rev. Genet.* **10**, 94–108 (2009).
4. Kim, V.N., Han, J. & Siomi, M.C. Biogenesis of small RNAs in animals. *Nat. Rev. Mol. Cell Biol.* **10**, 126–139 (2009).
5. Tsai, H.Y. *et al.* A ribonuclease coordinates siRNA amplification and mRNA cleavage during RNAi. *Cell* **160**, 407–419 (2015).
6. Pak, J., Maniar, J.M., Mello, C.C. & Fire, A. Protection from feed-forward amplification in an amplified RNAi mechanism. *Cell* **151**, 885–899 (2012).
7. Zhang, C. & Ruvkun, G. New insights into siRNA amplification and RNAi. *RNA Biol.* **9**, 1045–1049 (2012).
8. Pak, J. & Fire, A. Distinct populations of primary and secondary effectors during RNAi in *C. elegans*. *Science* **315**, 241–244 (2007).
9. Aoki, K., Moriguchi, H., Yoshioka, T., Okawa, K. & Tabara, H. In vitro analyses of the production and activity of secondary small interfering RNAs in *C. elegans*. *EMBO J.* **26**, 5007–5019 (2007).
10. Sijen, T., Steiner, F.A., Thijssen, K.L. & Plasterk, R.H. Secondary siRNAs result from unprimed RNA synthesis and form a distinct class. *Science* **315**, 244–247 (2007).
11. Yigit, E. *et al.* Analysis of the *C. elegans* Argonaute family reveals that distinct Argonautes act sequentially during RNAi. *Cell* **127**, 747–757 (2006).
12. Gu, W. *et al.* Distinct argonaute-mediated 22G-RNA pathways direct genome surveillance in the *C. elegans* germline. *Mol. Cell* **36**, 231–244 (2009).
13. Fischer, S.E. *et al.* The ERI-6/7 helicase acts at the first stage of an siRNA amplification pathway that targets recent gene duplications. *PLoS Genet.* **7**, e1002369 (2011).
14. Guang, S. *et al.* An Argonaute transports siRNAs from the cytoplasm to the nucleus. *Science* **321**, 537–541 (2008).
15. Shirayama, M., Stanney, W. III, Gu, W., Seth, M. & Mello, C.C. The Vasa Homolog RDE-12 engages target mRNA and multiple argonaute proteins to promote RNAi in *C. elegans*. *Curr. Biol.* **24**, 845–851 (2014).
16. Yang, H. *et al.* The DEAD box helicase RDE-12 promotes amplification of RNAi in cytoplasmic foci in *C. elegans*. *Curr. Biol.* **24**, 832–838 (2014).
17. Gu, W., Claycomb, J.M., Batista, P.J., Mello, C.C. & Conte, D. Cloning Argonaute-associated small RNAs from *Caenorhabditis elegans*. *Methods Mol. Biol.* **725**, 251–280 (2011).
18. Zhou, X. *et al.* Nuclear RNAi contributes to the silencing of off-target genes and repetitive sequences in *Caenorhabditis elegans*. *Genetics* **197**, 121–132 (2014).
19. Claycomb, J.M. *et al.* The Argonaute CSR-1 and its 22G-RNA cofactors are required for holocentric chromosome segregation. *Cell* **139**, 123–134 (2009).
20. Buckley, B.A. *et al.* A nuclear Argonaute promotes multigenerational epigenetic inheritance and germline immortality. *Nature* **489**, 447–451 (2012).
21. Batista, P.J. *et al.* PRG-1 and 21U-RNAs interact to form the piRNA complex required for fertility in *C. elegans*. *Mol. Cell* **31**, 67–78 (2008).
22. Gabel, H.W. & Ruvkun, G. The exonuclease ERI-1 has a conserved dual role in 5.8S rRNA processing and RNAi. *Nat. Struct. Mol. Biol.* **15**, 531–533 (2008).

23. Ni, J.Z. *et al.* A transgenerational role of the germline nuclear RNAi pathway in repressing heat stress-induced transcriptional activation in *C. elegans*. *Epigenetics Chromatin* **9**, 3 (2016).
24. Weick, E.M. *et al.* PRDE-1 is a nuclear factor essential for the biogenesis of Ruby motif-dependent piRNAs in *C. elegans*. *Genes Dev.* **28**, 783–796 (2014).
25. Ashe, A. *et al.* piRNAs can trigger a multigenerational epigenetic memory in the germline of *C. elegans*. *Cell* **150**, 88–99 (2012).
26. Shirayama, M. *et al.* piRNAs initiate an epigenetic memory of nonself RNA in the *C. elegans* germline. *Cell* **150**, 65–77 (2012).
27. Yi, Y.H. *et al.* A Genetic Cascade of let-7-ncl-1-fib-1 Modulates Nucleolar Size and rRNA Pool in *Caenorhabditis elegans*. *PLoS Genet.* **11**, e1005580 (2015).
28. Lee, L.W., Lee, C.C., Huang, C.R. & Lo, S.J. The nucleolus of *Caenorhabditis elegans*. *J. Biomed. Biotechnol.* **2012**, 601274 (2012).
29. Thompson, O. *et al.* The million mutation project: a new approach to genetics in *Caenorhabditis elegans*. *Genome Res.* **23**, 1749–1762 (2013).
30. Chen, X. *et al.* Dual sgRNA-directed gene knockout using CRISPR/Cas9 technology in *Caenorhabditis elegans*. *Sci. Rep.* **4**, 7581 (2014).
31. Astuti, D. *et al.* Germline mutations in DIS3L2 cause the Perlman syndrome of overgrowth and Wilms tumor susceptibility. *Nat. Genet.* **44**, 277–284 (2012).
32. Morris, M.R., Astuti, D. & Maher, E.R. Perlman Syndrome: overgrowth, Wilms tumor predisposition and DIS3L2. *Am. J. Med. Genet. C. Semin. Med. Genet.* **163C**, 106–113 (2013).
33. Chang, H.M., Triboulet, R., Thornton, J.E. & Gregory, R.I. A role for the Perlman syndrome exonuclease Dis3l2 in the Lin28-let-7 pathway. *Nature* **497**, 244–248 (2013).
34. Faehnle, C.R., Walleshauser, J. & Joshua-Tor, L. Mechanism of Dis3l2 substrate recognition in the Lin28-let-7 pathway. *Nature* **514**, 252–256 (2014).
35. Lubas, M. *et al.* Exonuclease hDIS3L2 specifies an exosome-independent 3′-5′ degradation pathway of human cytoplasmic mRNA. *EMBO J.* **32**, 1855–1868 (2013).
36. Malecki, M. *et al.* The exoribonuclease Dis3L2 defines a novel eukaryotic RNA degradation pathway. *EMBO J.* **32**, 1842–1854 (2013).
37. Bühler, M., Spies, N., Bartel, D.P. & Moazed, D. TRAMP-mediated RNA surveillance prevents spurious entry of RNAs into the *Schizosaccharomyces pombe* siRNA pathway. *Nat. Struct. Mol. Biol.* **15**, 1015–1023 (2008).
38. Lee, H.C. *et al.* qiRNA is a new type of small interfering RNA induced by DNA damage. *Nature* **459**, 274–277 (2009).
39. Cao, M. *et al.* Virus infection triggers widespread silencing of host genes by a distinct class of endogenous siRNAs in *Arabidopsis*. *Proc. Natl. Acad. Sci. USA* **111**, 14613–14618 (2014).
40. Zhang, Q., Shalaby, N.A. & Buszczak, M. Changes in rRNA transcription influence proliferation and cell fate within a stem cell lineage. *Science* **343**, 298–301 (2014).
41. Hokii, Y. *et al.* A small nucleolar RNA functions in rRNA processing in *Caenorhabditis elegans*. *Nucleic Acids Res.* **38**, 5909–5918 (2010).
42. Feng, X. & Guang, S. Small RNAs, RNAi and the inheritance of gene silencing in *Caenorhabditis elegans*. *J. Genet. Genomics* **40**, 153–160 (2013).
43. Guang, S. *et al.* Small regulatory RNAs inhibit RNA polymerase II during the elongation phase of transcription. *Nature* **465**, 1097–1101 (2010).
44. Mao, H. *et al.* The Nrde pathway mediates small-RNA-directed histone H3 lysine 27 trimethylation in *Caenorhabditis elegans*. *Curr. Biol.* **25**, 2398–2403 (2015).
45. Lim, J. *et al.* Uridylation by TUT4 and TUT7 marks mRNA for degradation. *Cell* **159**, 1365–1376 (2014).
46. Slevin, M.K. *et al.* Deep sequencing shows multiple oligouridylations are required for 3′ to 5′ degradation of histone mRNAs on polyribosomes. *Mol. Cell* **53**, 1020–1030 (2014).
47. Łabno, A. *et al.* Perlman syndrome nuclease DIS3L2 controls cytoplasmic non-coding RNAs and provides surveillance pathway for maturing snRNAs. *Nucleic Acids Res.* **44**, 10437–10453 (2016).
48. Dammel, C.S. & Noller, H.F. A cold-sensitive mutation in 16S rRNA provides evidence for helical switching in ribosome assembly. *Genes Dev.* **7**, 660–670 (1993).
49. Girard, J.P., Feliu, J., Caizergues-Ferrer, M. & Lapeyre, B. Study of multiple fibrillarin mRNAs reveals that 3′ end formation in *Schizosaccharomyces pombe* is sensitive to cold shock. *Nucleic Acids Res.* **21**, 1881–1887 (1993).
50. Spithill, T.W., English, K.J., Nagley, P. & Linnane, A.W. Altered mitochondrial ribosomes in a cold-sensitive mutant of *Saccharomyces cerevisiae*. *Mol. Biol. Rep.* **4**, 83–86 (1978).
51. Stevens, R.H. & Amos, H. RNA metabolism in HeLa cells at reduced temperature. I. Modified processing of 45S RNA. *J. Cell Biol.* **50**, 818–829 (1971).
52. Tashiro, K., Misumi, Y., Shiokawa, K. & Yamana, K. Determination of the rate of rRNA synthesis in *Xenopus laevis* triploid embryos produced by low-temperature treatment. *J. Exp. Zool.* **225**, 489–495 (1983).
53. Xia, B., Ke, H., Shinde, U. & Inouye, M. The role of RbfA in 16S rRNA processing and cell growth at low temperature in *Escherichia coli*. *J. Mol. Biol.* **332**, 575–584 (2003).
54. Duchaine, T.F. *et al.* Functional proteomics reveals the biochemical niche of *C. elegans* DCR-1 in multiple small-RNA-mediated pathways. *Cell* **124**, 343–354 (2006).

ONLINE METHODS

Strains. Bristol strain N2 was used as the standard wild-type strain. The Hawaiian strain CB4856 was used for snip-SNP mapping. All strains were incubated at 20 °C. The strains used in this study are listed in **Supplementary Table 4**.

RNAi. RNAi experiments were conducted as described previously[55]. HT115 bacteria expressing the empty vector L4440 (a gift from A. Fire) were used as controls. dsRNA targeting the 18S and 26S rRNA were PCR amplified with the primer pairs 18S-F-5′-TTTAAGCTTCTCTATCCGGAAAGGGTG-3′ and 18S-R-5′- TTTAAGCTTCGGTATCTAATCGCCTTC-3′, 26S-F-5′-TTTAAGCTTGCGGCACTGTTGGTTCGC-3′ and 26S-R-5′- TTTAAGCTTGGCTTCATCCTGCTCAGG-3′, respectively, from N2 genomic DNA, digested with HindIII, inserted into L4440, and transformed into the HT115 *E. coli* strain (underlining indicates recognition sequences of the restriction enzymes).

Images were collected on Zeiss Imager D1 microscope and Leica DM2500 microscope.

Quantification of the subcellular location of NRDE-3. *C. elegans* has 16 seam cells at L4 stage. In wild-type N2 animals, the majority of NRDE-3 localizes in the nucleus in all 16 seam cells[14]. In *eri-1(mg366)* animals, the majority of NRDE-3 accumulates in the cytoplasm in all 16 seam cells. The nuclear localization of NRDE-3 can be restored by *susi-1* mutation in the *eri-1(mg366);susi-1(ust1)* double mutant. A nuclear (N) phenotype was assigned to an individual animal if one or more out of a total of 16 seam cells showed a clear nuclear enrichment in the indicated genetic background. The relative nuclear and cytoplasmic signal intensity were not taken into consideration at this work. In wild-type N2 and *eri-1(mg366);susi-1(ust1)* animals, NRDE-3 localizes to the nucleus in all 16 seam cells (100% N). In *eri-1(mg366)* animals, NRDE-3 localizes to the cytoplasm in all 16 seam cells (0% N).

Construction of plasmids and transgenic strains. For *nrde-3p::FLAG::gfp::susi-1*, a 2.2 kb *nrde-3* promoter region was PCR amplified with the primers 5′-TTTAAGCTTTTTTCCATACATTGCTCTTCG- 3′ and 5′- AAAAAGCTTGAGATCCATGATTAGTTGTGC-3′, and inserted into the HindIII site of pRP2512. The 3xFLAG::GFP coding region was PCR amplified from YY174: *3xflag::gfp::nrde-3 (ggIS1)* genomic DNA with the primers 5′-TTTGTCGACATGGACTACAAAGACCATGACGGTGATTATAAAGATCATGATATCGATTACAAGGATGACGATGACAAGATGAGTAAAGGAGAAGAACTTTTC -3′ and 5′-AAAGTCGACTTTGTATAGTTCATCC-3′, digested with SalI, and inserted into XhoI site of pRP2512. The coding region and 3′ UTR of *susi-1* were PCR amplified with the primers 5′-CGGGGTACCATGTCAGCAGTTGAAAGTCCCGTTATTGTG-3′ and 5′-CGGGGTACCGGATCTTCTCTCGGCGATGCTCGTCTGTC-3′, and inserted into the KpnI site of pRP2512 to make *nrde-3p::3x FLAG::gfp::susi-1* fusion protein (underlining indicates recognition sequences of the restriction enzymes). The transgene was integrated onto the *C. elegans* genome by microparticle bombardment.

For *susi-1p::mCherry::susi-1*, a 2.3-kb *susi-1* promoter region was PCR amplified with the primers 5′-CCCAAGCTTGGTGGAATGAAGGAGATATATG-3′ and 5′- CCCAAGCTTCTAGAATAAATGGTAATTTGGGGG-3′, and inserted into the HindIII site of pRP2512. The mCherry coding region was PCR amplified from SX333 with the primers 5′- CCAAATTACCATTTATTCTAGAAGCTTATGGTGAGCAAGGGCGAGGAGG-3′ and 5′- GACTTTCAACTGACATGGTACCCTTGTACAGCTCGTCCATGCCG-3′. The coding region and 3′ UTR of *susi-1* were PCR amplified with the primers 5′-GGTACCATGTCAGCAGTTGAAAGTCCCGTTATTGTG-3′ and 5′-CGGGGTACCGGATCTTCTCTCGGCGATGCTCGTCTGTC-3′. The mCherry and *susi-1* coding region were cloned into the pRP2512 with a homologous recombination kit (Vazyme C113-02) to generate the *susi-1p::mCherry::susi-1* fusion gene.

For risiRNA sensor, a 1 kb *his-72* promoter sequence was PCR amplified with the primers 5′-CCCAAGCTTGATGATATTTCAACCGGAGAACC-3′ and 5′-CCCAAGCTTCACGACGACAAACAGAACAACTG-3′, and inserted into the HindIII site of pRP2512. *his-72* coding region was PCR amplified with the primers 5′-CGGGGTACCATGAGAGGTGCGTGCGTGTGC-3′ and 5′-CGGGGTACCCACGGACAAATACATCGGTTTTACAAC-3′. 3xFLAG::GFP coding region was PCR amplified from YY174 genomic DNA as described above. A 120-nt 26S rRNA fragment was PCR amplified with the primers 5′-CTGAACGCCTCTAAGTTAGAATC-3′ and 5′-TTAGCCAAGGCCATACATAGGGCAT-3′. The 3′ UTR of *his-72* was PCR amplified with the primers 5′-ATGCCCTATGTATGGCCTTGGCTAAGCTCCATCACCAATTCTCGAAGC-3′ and 5′-CGGGGTACCCACGCAACGCGCCGTAAACCTACAC-3′. These four fragments, *his-72 cds*, *gfp*, 26S rRNA and *his-72 utr*, were then fused by fusion PCR and inserted into the KpnI site of pRP2512 to make a *his-72p::3x FLAG::GFP::his-72::rRNA* fusion gene (underlining indicates recognition sequences of the restriction enzymes). The transgene was integrated into the *C. elegans* genome by microparticle bombardment.

For *mCherry::FIB-1*, the mCherry coding region was PCR amplified from SX333 with the primers: 5′-GTAGTATGGGACGTCCAGAGATGGTGAGCAAGGGCGAGGAGG-3′ and 5′- CTTGTACAGCTCGTCCATGCCG-3′. A 1.8-kb *fib-1* promoter region was PCR amplified with the primers 5′-ATACGACTCACTAGTGGGCAGGGTGAACAGCGCGAATTGATCTCCAGTC-3′ and 5′- CTCTGGACGTCCCATACTACAAAAATCG-3′. The coding region and 3′ UTR of *fib-1* were PCR amplified with the primers: 5′- CGGCATGGACGAGCTGTACAAGATGGGACGTCCAGAGTTCAATCG-3′ and 5′- CTACGTAATACGACTCACTTGCTCTAAACCAATACAACAATTCG-3′. These three fragments were cloned into pCFJ151 with a Homologous recombination kit (Vazyme C113-02) to make *fib-1p::mCherry::FIB-1* fusion gene. The transgene was further integrated into *C. elegans* genome by mos1-mediated single copy insertion (MosSCI).

Genetic screening. To identify factors that can negatively regulate endo-siRNA generation, we screened for mutants that redistribute NRDE-3 from the cytoplasm to the nucleus in *eri-1(mg366);gfp::nrde-3* animals. In *eri-1(mg366)* mutant, NRDE-3 localizes in the cytoplasm in the absence of binding to endo-siRNA. *eri-1(mg366);gfp::nrde-3* animals were mutagenized by ethyl methanesulfonate (EMS), followed by a clonal screening with 8,000 haploid genomes. The F2 progeny worms were visualized under a fluorescence microscope at L3/L4 stage. Mutants that redistribute NRDE-3 to the nucleus were selected. We isolated 39 mutants in which GFP::NRDE-3 accumulated in the nucleus. Eight mutants were viable and stably maintained the phenotype. *susi-1* was identified by snip-SNP mapping followed by sequencing of the genome.

Dual sgRNA-directed *susi-1* deletion. Dual sgRNA-guided chromosome deletion was conducted as previously described[30]. We manually searched for target sequences consisting of $G(N)_{19}NGG$ near the desired mutation sites in *susi-1* genomic region. We replaced the *unc-119* target sequence in the pU6::unc-119 sgRNA vector with the desired target sequence using overlapped extension PCR by primer pairs sgRNA-1F: GAGAAAAAACGTGGAATGGGTTTTAGAGCTAGAAATAGC and sgRNA-1R: CCATTCCACGTTTTTTCTCCAAACATTTAGATTTGCAATTC; sgRNA-2F: GAATATGTGAAATGGTGGGGTTTTAGAGCTAGAAATAGC and sgRNA-2R: CCCACCATTTCACATATTCCAAACATTTAGATTTGCAATTC. Plasmid mixtures containing 50 ng/μl sgRNA-1, 50 ng/μl sgRNA-2, 50 ng/μl Cas9 expression plasmid, 5 ng/μl pCFJ90 and 5 ng/μl pCFJ104 were co-injected into YY178: *eri-1(mg366);3xflag:: gfp::nrde-3(ggIS1)*. The deletion mutants were screened by PCR amplification.

Low-temperature treatment. Synchronized embryos or L3/L4 animals were incubated at 20 °C, 15 °C or 4 °C for 12 h, then grown at 20 °C for 2 h, followed by counting, photographing, and RNA isolation and quantification.

UV irradiation. Synchronized embryos or L3/L4 animals were irradiated by Ultraviolet (HL-2000 HybriLinker) at indicated doses, then grown at 20 °C for 2 h, followed by counting, photographing, and RNA isolation and quantitation. A nuclear (N) phenotype was assigned to an individual embryo if half of the nuclei showed a clear nuclear enrichment of NRDE-3. The relative nuclear and cytoplasmic signal intensity were not taken into consideration.

Quantitative RT-PCR. RNAs were isolated from embryos using a dounce homogenizer (pestle B) in TRIzol solution followed by DNase I digestion (Qiagen), as described previously[14]. cDNAs were generated from RNAs using the iScript cDNA Synthesis Kit (Bio-Rad) according to the vendor's protocol. qPCR was performed using an MyIQ2 machine (Bio-Rad) with iQ SYBR Green Supermix (Bio-Rad). The primers for pre-mRNA analysis that were used in qRT-PCR are listed in **Supplementary Table 5**. *eft-3* mRNA was used as an

doi:10.1038/nsmb.3376

control for sample normalization. The data analysis was performed using a comparative threshold cycle (ΔΔCT) approach.

TaqMan assay. risiRNAs were reverse transcribed with a microRNA reverse-transcription kit (4366596; Applied Biosystems). cDNAs were quantified by RT-PCR using custom small RNA TaqMan assays from Applied Biosystems (4398987; assay IDs CSKAJ28 and CSKAJ28) to detect the following small RNA sequences: 26S risiRNA 5′-GAGAUAGAGAUGCCUCCCGACA-3′ and 18S risiRNA 5′-GGCAAAUGCUUUCGCUGUUGGG-3′.

RNA immunoprecipitation (RIP). RIP experiments were performed as previously described with hypochlorite-isolated embryos[14]. Briefly, the embryos were sonicated in lysis buffer (20 mM Tris-HCl (pH 7.5), 200 mM NaCl, 2.5 mM MgCl2, and 0.5% NP-40); the lysate was pre-cleared with protein G–agarose beads (Roche), and incubated with anti-FLAG M2 agarose beads (Sigma #A2220). The beads were washed extensively, and 3xFLAG::GFP::NRDE-3 and associated RNAs were eluted with 100 μg/ml 3xFLAG peptide (Sigma). The eluates were incubated with TRIzol reagent (Invitrogen), followed by isopropanol precipitation. NRDE-3-bound RNAs were quantified by real-time PCR.

Isolation and sequencing of NRDE-3-associated small RNAs. NRDE-3-associated siRNAs were isolated from embryo lysates as previously described[14]. Briefly, the animals were sonicated in lysis buffer (20 mM Tris-HCl (pH 7.5), 200 mM NaCl, 2.5 mM $MgCl_2$, and 0.5% NP-40); the lysate was pre-cleared with protein G–agarose beads (Roche), and incubated with anti-FLAG M2 agarose beads. The beads were washed extensively, and 3xFLAG::GFP::NRDE-3 and associated RNAs were eluted with 100 μg/ml 3xFLAG peptide. The eluates were incubated with TRIzol reagent (Invitrogen), followed by isopropanol precipitation. The precipitated RNAs were treated with calf intestinal alkaline phosphatase (CIAP, Invitrogen), re-extracted with TRIzol, and treated with T4 polynucleotide kinase (T4 PNK, New England BioLabs) in the presence of 1 mM ATP or [γ-^{32}P]ATP for labeling.

The NRDE-3-associated siRNAs were manually cloned and sequenced as described previously[14].

Biochemical characterization of risiRNA. The capping assay was performed as described previously[14]. Briefly, NRDE-3-associated risiRNAs were immunoprecipitated from bleached embryos, purified, and then catalyzed by guanylyl transferase (Ambion) in the presence of m^7G according to the manufacturer's instructions. The products were further dephosphorylated by calf intestinal alkaline phosphatase (CIAP) and labeled by T4 polynucleotide kinase (T4 PNK) in the presence of [γ-^{32}P]ATP. If a siRNA carries 5′ di- or triphosphate groups, the guanylyl transferase will add m^7G to its 5′ end, which protect the RNA from downstream CIAP treatment and T4 PNK labeling.

The β-elimination assay was conducted as described previously[14]. Briefly, NRDE-3-associated risiRNAs were immunoprecipitated from bleached embryos, purified, dephosphorylated by CIAP, and then labeled by T4 PNK in the presence of [γ-^{32}P]ATP. The products were treated by β-elimination in the presence of 100 mM sodium periodate at room temperature for 10 min, boiled in formamide loading dye for 30 min, and then separated by PAGE electrophoresis.

Deep sequencing of small RNAs and bioinformatics. Total siRNAs were isolated from embryo lysates and subjected to deep sequencing using an Illumina platform, according to the manufacturer's instructions, by the Beijing Genomics Institute (BGI Shenzhen). Small RNAs ranging from 18 to 30 nt were gel purified and ligated to a 3′ adaptor (5′-pUCGUAUGCCGUCUUCUGCUUGidT-3′; p, phosphate; idT, inverted deoxythymidine) and a 5′ adaptor (5′-GUUCAGAGUUCUACAGUCCGACGAUC-3′). The ligation products were gel purified, reverse transcribed and amplified using Illumina's sRNA primer set (5′-CAAGCAGAAGACGGCATACGA-3′; 5′-AATGATACGGCGACCACCGA-3′). The samples were then sequenced using an Illumina Hiseq platform.

The Illumina-generated raw reads were first filtered to remove adaptors, low-quality tags and contaminants to get clean reads at BGI Shenzhen. Clean reads ranging from 18 to 30 nt were mapped to the unmasked *C. elegans* genome and the transcriptome assembly WS243, respectively, using Bowtie2 with default parameters[56]. The number of reads targeting each transcript was counted by custom Perl scripts and displayed by IGV[57]. The number of total reads mapped to the genome minus the number of total reads corresponding to sense rRNA transcripts (5S, 5.8S, 18S and 26S) was used as the normalization number, to exclude the possible degradation fragments of sense rRNAs.

TAIL-seq. Total RNAs were extracted from embryos, digested by DNase I, and then ligated to the following 3′ RNA linkers with T4 RNA ligase (Thermo #EL0021) (300 ng total RNAs, 2 μl 3′ RNA linker (10 ng/μl), 1μl 10× T4 RNA ligation buffer, 2 μl T4 RNA ligase, 37 °C, 30 min).

3′ RNA linker-1: 5′-pGATCCACACTCGGGCACCAAGGATTTAACCGCGAATTCCAGC-NH2-3′ (the underlined sequence served as a barcode for sample labeling).

3′ RNA linker-2: 5′-pGTACCACACTCGGGCACCAAGGATTTAACCGCGAATTCCAGC-NH2-3′.

3′ RNA linker-3: 5′-pCGACACACTCGGGCACCAAGG-NH2-3′.

The RNAs were reverse transcribed with the following primers:

3′ linker RT-1: 5′-GCTGGAATTCGCGGTTAAATCCTTGGTGCCCGAGTGTGGATC-3′.

3′ linker RT-2: 5′-GCTGGAATTCGCGGTTAAATCCTTGGTGCCCGAGTGTGGTAC-3′.

3′ linker RT-3: 5′-GCTGGAATTCGCGGTTAAATCCTTGGTGCCCGAGTGTGTCG-3′.

The cDNAs were PCR amplified with the primers 26S rRNA-202-F: 5′-CATCTCTATCTCGTGGCAACACGAG-3′ and linker-R: 5′-GCTGGAATTCGCGGTTAAATCCTTG-3′, gel purified and then deep sequenced using an Illumina platform, according to the manufacturer's instructions, by the Beijing Genomics Institute (BGI Shenzhen). The number of reads with distinct 3′-end modifications were counted by custom Perl scripts.

RNA injection. Single-stranded 26S rRNA (101 nt in length; named 101 nt + 0U) (CACUUGCAUACGACUUGGUCUCUUGGUCAAGGUGUUGUAUUCAGUAGAGCAGUCCUUUUAUACUGCGAUCUGUUGAGACUAUCCUUUGAUUGAGUUUUUUG) and 26S rRNA with 6 additional uridine (101 nt + 6U) (CACUUGCAUACGACUUGGUCUCUUGGUCAAGGUGUUGUAUUCAGUAGAGCAGUCCUUUUAUACUGCGAUCUGUUGAGACUAUCCUUUGAUUGAGUUUUUUGUUUUUU) were synthesized with T7 RNA polymerase *in vitro* (Thermo Kit #K0441), digested by DNase I, and then purified by PAGE gel system. L3/L4 animals were selected for microinjection with the RNAs at a concentration of 100 ng/μl. The injected animals were photographed 90 min later.

Statistics. Bar graphs with error bars show mean and s.d. Statistical analysis was performed with two-tailed Student's *t*-test. No statistical method was used to predetermine sample size; experiments were not randomized and were not performed with blinding.

Data availability. The next-generation sequencing data discussed in this publication have been deposited in NCBI's Gene Expression Omnibus[58] and are accessible through GEO Series accession number GSE90927. Argonaute-associated small RNAs from published data were reanalyzed: CSR-1 immunoprecipitation (IP), SRR030753 (ref. 19); HRDE-1 IP, SRR498193 (ref. 20); WAGO-1 IP, SRR030711 (ref. 12); PRG-1 IP, GSM297758 ref. 21); NRDE-3 immunoprecipitation and deep sequencing, GSE92307 (ref. 18). Total small RNA of published mutants was also analyzed: *hrde-1(tm1200)*, SRR2832559 (ref. 23); *mago12*, SRR030713 (ref. 12); *prg-1(n4357)*, GSM1195517 (ref. 24). Source data for **Figures 2–8** and **Supplementary Figures 1–8** are available online. All other data and materials are available from the corresponding author upon request.

55. Timmons, L., Court, D.L. & Fire, A. Ingestion of bacterially expressed dsRNAs can produce specific and potent genetic interference in *Caenorhabditis elegans*. *Gene* **263**, 103–112 (2001).
56. Langmead, B. & Salzberg, S.L. Fast gapped-read alignment with Bowtie 2. *Nat. Methods* **9**, 357–359 (2012).
57. Thorvaldsdóttir, H., Robinson, J.T. & Mesirov, J.P. Integrative Genomics Viewer (IGV): high-performance genomics data visualization and exploration. *Brief. Bioinform.* **14**, 178–192 (2013).
58. Edgar, R., Domrachev, M. & Lash, A.E. Gene Expression Omnibus: NCBI gene expression and hybridization array data repository. *Nucleic Acids Res.* **30**, 207–210 (2002).